NASA-TM-111258

AIAA-95-2277

A PARAMETRIC STUDY OF SUPERSONIC LAMINAR FLOW FOR SWEPT WINGS USING LINEAR STABILITY ANALYSIS

Joseph A. Garcia and Eugene L. Tu
NASA Ames Research Center
Moffett Field, CA

Russell M. Cummings
California Polytechnic State University
San Luis Obispo, CA

26th AIAA Fluid Dynamics Conference
June 19–22, 1995 / San Diego, CA

A Parameteric Study of Supersonic Laminar Flow for Swept Wings Using Linear Stability Analysis

Joseph A Garcia* and Eugene L. Tu†
NASA Ames Research Center
Moffett Field, CA 94035

Russell M. Cummings‡
California Polytechnic State University
San Luis Obispo, CA 93407

Abstract

A parametric study to predict the extent of laminar flow on the upper surface of a generic swept-back wing (NACA 64A010 airfoil section) at supersonic speeds was conducted. The results were obtained by using surface pressure predictions from an Euler/Navier-Stokes computational fluid dynamics code coupled with a boundary-layer code, which predicts detailed boundary-layer profiles, and finally with a linear stability code to determine the extent of laminar flow. The parameters addressed are Reynolds number, angle of attack, and leading-edge wing sweep. The results of this study show that an increase in angle of attack, for specific Reynolds numbers, can actually delay transition. Therefore, higher lift capability, caused by the increased angle of attack, as well as a reduction in viscous drag due to the delay in transition is possible for certain flight conditions.

Introduction

Laminar flow control has been identified as a key element in the development of the next generation of High Speed Civil Transports. Extending the amount of laminar flow over an aircraft will increase range, payload and altitude capabilities as well as lower skin temperature. All these benefits translate into lower fuel requirements and overall cost. A major design parameter for future supersonic transport aircraft is aerodynamic efficiency. Aerodynamic efficiency, which contributes significantly to the aircraft's fuel efficiency, can be improved through increases in cruise lift and/or decreases in total drag. Turbulent skin friction, in particular, is known to contribute a large portion of the aircraft's total drag. Therefore, techniques to increase the extent of laminar flow, which reduces skin friction, can result in significant improvements in aerodynamic efficiency and, as a result, savings in fuel costs.

Until recently, most studies on laminar flow have been in the subsonic flow region. Work done in this regime has shown that turbulent skin friction drag can contribute as much as 50% of the total aircraft drag.[4] Furthermore, studies on typical supersonic transports (SST) and transonic aircraft have shown significant potential to increase the cruise lift-to-drag ratio by increasing the extent of laminar flow.[2-3] Another benefit of laminar flow at supersonic speeds includes a reduction in aerodynamic heating which allows for more skin/structure material options and, therefore, decreased aircraft gross weight and increased range/payload capability.

In most cases, increasing the extent of laminar flow is equivalent to delaying boundary-layer transition, which can be achieved by passive or active techniques.[4] Passive techniques, also known as Natural Laminar Flow (NLF) control, alter the boundary-layer flow through normal aerodynamic control parameters (e.g., wall shaping, surface smoothing, angle of attack, Reynolds number). Active techniques alter the flow using external means (e.g., wall suction and heat transfer).

Boundary-layer transition is composed of several physical processes as described in Fig. 1 (taken from Ref. 4). The transition process begins by introducing external disturbances into the boundary layer through a viscous process know as "receptivity."[5] Some of these external disturbances include freestream vorticity, surface roughness, vibrations and sound. Identifying and defining the initialization of these external disturbances, for a given problem, is the basis for the prediction of transition and creates an initial boundary-value problem. The initial disturbance is a function of the type of flow in consideration as well as its environment and therefore is not usually known.[4]

* Aerospace Engineer, Applied Computational Aerodynamics Branch. Formerly Graduate Research Assistant, Aeronautical Engineering Department, California Polytechnic State University, San Luis Obispo. Member AIAA.
† Aerospace Engineer, Applied Computational Aerodynamics Branch. Member AIAA.
‡ Department Chair and Professor. Associate Fellow AIAA.

The disturbances in the boundary-layer eventually amplify and can be modeled by linear stability theory. The normal modes responsible for the amplification of these disturbances in the boundary-layer flow are the viscous Tollmein Schlichting (T-S) waves, inflectional Rayleigh waves (i.e., instabilities due to crossflow), and Görtler vortices for curved streamlines.[4] Once the amplifications are large enough, nonlinearity sets in through secondary and tertiary instabilities and the flow becomes "transitional".[4] It should be noted that the nonlinear portion of the flow is small compared to the linear region and therefore can still often be approximated by linear stability theory for preliminary designs.

One thing that must be avoided is the introduction of high levels of initial nonlinear disturbances, which cause a bypass of the linear disturbance regime and yields an almost instantaneous transition. An example of such a nonlinear transition is attachment-line contamination, commonly found in swept wings caused by turbulent flow from the fuselage.

The common normal modes found on a swept wing are T-S and crossflow. The effect of sweeping the wing introduces a three-dimensional crossflow instability created by a high pressure gradient near the wing leading edge that eliminates the ability to maintain laminar flow. The sweep and adverse pressure gradient near the trailing edge likewise induces crossflow instabilities on the trailing edge of the wing. Furthermore, the "viscous" two dimensional Tollmein Schlichting (TS) instabilities are damped when a favorable pressure gradient is applied, while the three-dimensional crossflow "inflectional" instabilities are amplified when such pressure gradients exist.[6]

Computational Method

The results in this study were obtained by the combination of an advanced computational fluid dynamics (CFD) code, a boundary-layer code, and a boundary-layer stability code.

The CFD code, specifically the NASA Ames three dimensional Compressible Navier Stokes (CNS) code, solves the Euler or thin-layer Navier-Stokes equations using finite difference and uses one of two algorithm options. These options are the implicit approximation factorization algorithm in delta form by Beam and Warming[10] and the diagonal implicit algorithm by Pulliam and Chaussee.[11] The Pulliam-Chaussee diagonal algorithm was used for all mean flow computations in the present study. The solid wall conditions are specified in CNS as no-slip and adiabatic for the Navier Stokes equations. The outer boundary or far field flow variables are set to free stream flow conditions and the downstream boundary is set to outflow conditions. Finally, a symmetry condition is used at the wing root to eliminate effects due to the fuselage that could result in leading-edge flow contamination.

Due to the extensive amount of computer time required by the CNS code to obtain accurate boundary-layer results, only one case was converged to this point in order to compare boundary-layer results with those obtained by the boundary-layer code. All other cases were converged to provide only the accurate pressure distribution over the wing surface. Accurate predictions of pressures for similar geometries and conditions have been demonstrated in previous studies.[12]

The surface pressure results from the CNS code are used to compute detailed boundary-layer profiles through the use of the "Kaups and Cebeci" compressible boundary-layer code (WING).[8] The WING code uses a conical flow approximation valid for pressure isobars along constant percent chord lines for wings of trapezoidal planforms.[8] It should be noted that this assumption is not valid near the tip or root of the wing due to the strong pressure gradients created in these locations. The boundary-layer code WING uses the Keller box method to solve the boundary-layer equations. This method has been proven to be an accurate and efficient method to solve parabolic partial differential equations of this type.[13-16]

Next, the boundary-layer results are supplied to the three-dimensional Compressible Stability AnaLysis (COSAL) code to predict transition.[9] The COSAL code uses small-disturbance theory[17] to analyze the stability of the three-dimensional boundary layer in order to predict transition and has been validated in several previous studies.[18-19] The two type of instabilities that COSAL can compute are Tollmein Schlichting (TS) or crossflow. Note, only one of the two modes can be analyzed at one time and for this study crossflow was used. The COSAL code uses a second-order finite-difference formulation and includes two eigenvalue search procedures[20] to solve the stability equations. A global eigenvalue search procedure is used when no guess is available for the eigenvalues. A local eigenvalue search is used, which is approximately 10 times faster than the global procedure,[20] when a good guess to the eigenvalues is available.

Finally, in order to conduct the following parametric study it was necessary to automate the analysis process due to the extensive number of interactive hours required to obtain a three dimensional transition prediction. As a result of the automated process the amount of interactive time required to obtain a single three-dimensional transition front has dropped from days to a matter of hours. A copy of the script can be found in Ref. 21 along with more details of the process. Using the automated stability process, a search of 23 frequencies for 8 selected span stations on a wing requires a total average CPU time of 1.5 hours on a single processor Cray Y-MP.

Furthermore, it was determined that the stability analysis must be run with 64 bit precision due to the needed accuracy of the eigenvalue search routine used in COSAL.

Computational Grids

The wing surface grids used in this analysis (see Fig. 2 for an example) were generated from an algebraic surface grid generation code developed in this study. The NACA 64A010 airfoil description was used to generate the wing surfaces. A three-dimensional C-H topology grid was generated using the hyperbolic volume grid generator, HYPGEN.[22] Note that the surface grid clustering near the leading edge (Fig. 2) was needed to capture the leading-edge effects critical for transition prediction. This required an initial spacing at the leading edge equal to .001 of the root chord. Also required was an initial spacing of 1E-6 in the wall normal direction, scaled by root chord, in order to have enough points to predict the boundary-layer profiles from the Navier Stokes solution. Recall, that these profiles were only used to compare with the profiles obtained by the boundary-layer solution. Hence for the Navier Stokes prediction a grid size of 157X36X75 in the streamwise, spanwise and wall normal direction, respectively, was used. For the Euler calculation only 55 points were used in the wall normal direction.

Results and Discussion

The parameters addressed in the present study are Reynolds number, angle of attack, and leading-edge wing sweep. Since this study is being focused on High Speed Civil Transport (HSCT) type aircraft, the range of angle of attack is limited to 0-10 degs. A base Reynolds number of 1.12 million per foot based on a Mach number of 1.5 and an altitude of approximately 45,000 feet is used. The leading-edge sweeps consist of 45 and 60 degs.

Boundary Layer Comparison

A comparison of boundary layer profiles obtained from the boundary-layer code WING (using CNS pressure predictions) with those computed directly from the Navier Stokes code (CNS) was conducted. All comparison are at the 48% semispan station. First, the edge velocity magnitude ($\sqrt{u_e^2+v_e^2+w_e^2}$), obtained from the two codes and normalized by the speed of sound (a_∞), were compared as shown in Fig. 3. Where, u_e, v_e and w_e are the edge velocities in the x-, y- and z-Cartesian direction, respectively. The two results agree well. Next, as illustrated in Figs. 4 and 5, the components of the boundary layer velocity in the x- and y-Cartesian directions, respectively, were compared for the x/c stations of 1%, 10% and 21%. The x-Cartesian velocity profiles (Fig. 4) show good agreement at all x/c stations while the y-Cartesian profiles (Fig. 5) show some discrepancies near the leading edge. This discrepancy is partially due to the lack of surface-normal orthogonality for the grid used in the Navier Stokes computation.

It is also noted that the initially computed boundary-layer thickness for the CNS prediction was originally much larger than shown in Figs. 4 and 5 and was attributed to the artificial dissipation introduced by the numerical computation of the Navier-Stokes equations. When numerical dissipation coefficients were lowered, and further convergence of the solutions obtained, the CNS comparisons with the WING results improved.

Reynolds Number Effects

The results of the Reynolds number study show that the extent of laminar flow decreases as the local Reynolds number increases. This is illustrated in Fig. 6 by the transition fronts of the chosen baseline wing for the Reynolds numbers of 6.34 million and 12.68 million. The light gray region signifies the portion of the wing where laminar flow is no longer predicted. The dark gray region represents laminar flow as predicted by the COSAL code for disturbance levels (N-factors) in the boundary layer below the value of 8. The N-factor can be described as the amplification measurement of the disturbances in a boundary layer of specific frequency and wave lengths. The disturbance level of 8, indicated by the solid black line, was chosen as the critical transition N-factor for all of the parameters addressed in this study. This disturbance level was selected based on previous swept wing transition prediction studies.[13-14]

The transition results near the tip and root of the wing were further investigated due to the conical flow assumption used in the boundary-layer code (WING). Investigation into the conical flow assumption showed that for this configuration the flow was not truly conical as seen in the pressure coefficient (Cp) plots of the two Reynolds number cases in Fig. 7. These plots show the upper chordwise pressure distribution versus the normalized x/c locations for the eight span station locations computed in the boundary-layer stability analysis. If the flow was truly conical, the Cp distribution for each span station would, when plotted against normalized local chord length, overlap. The Cp distribution results (Fig. 7) show that some conical flow does occur for approximately the first 20% chord between the 48% and 87% semispan stations. The Cp distributions also show that for the 33% semispan, conical flow is only valid up to approximately 10% chord. Finally, for the 13% to 19% semispan stations the conical flow assumption is not valid. Therefore, only the 48% semispan station of the wing will be discussed in detail.

Furthermore, the pressure distribution results (Fig. 7) show that there exists a strong favorable pressure

gradient at the leading-edge of the wing and a strong adverse pressure gradient at the wing's trailing edge which, as was mentioned in the introduction, amplify crossflow instabilities and damp out the T-S instabilities. Therefore, all boundary-layer stability calculations were conducted for crossflow instabilities only.

In order to study the flow more thoroughly, crossflow boundary-layer profile plots were made for the two Reynolds number cases at 48% semispan. Since transition is found to occur before 20% chord, crossflow boundary-layer profiles were plotted for x/c of 1, 10 and 21% as shown in Fig. 8. The crossflow profiles reveal that the magnitude of the maximum crossflow velocities remains the same and the inflection point of the profile moves closer to the wall as the Reynolds number is increased. Therefore, the boundary layer becomes thinner as the Reynolds number is increased. Note, since the Reynolds number is varied by changing the root chord of the wing, it was necessary to nondimensionalize the boundary-layer's normal distance from the wall (y) with the corresponding local chord (c) length in order to get a true comparison.

Figures 9 and 10 show the crossflow profiles and shear stress levels, respectively, normalized with boundary-layer thickness (δ) for the 10% chord location. Nondimensionalizing the normal distance y by δ shows that the inflection of the crossflow profiles now occur at the same y/δ for the two different Reynolds number cases as seen in Fig. 9. However, a plot of y/δ versus shear stress (Fig. 10), which is directly related to the viscosity in the boundary-layer, reveals that the shear stresses in the boundary layer are lower for the higher Reynolds number case and higher for the lower Reynolds number case, at a given y/δ. This inverse relation between shear stress and Reynolds number is attributed to the fact that Reynolds number was varied by changing the root chord. Finally, Figures 9 and 10 show that the crossflow boundary-layer is effectively in a higher viscosity region for the lower Reynolds number case.

Next, stability curves of the transition results at the 48% semispan station are shown in Fig. 11. This figure is a plot of chordwise x/c versus frequency for the Reynolds number study at the critical boundary-layer disturbance level (N-factor) of 8. The plot shows the x/c locations at which the given frequencies yield the disturbance level of 8. Transition is then predicted at the x/c value where this disturbance level first occurs. For example, for the Reynolds number of 6.3 million, the curve indicates that the disturbance level of 8 first occurs at the x/c value of approximately 12% for a frequency of 14000 Hz. For the higher Reynolds number case of 12.7 million, the results show that the transition shifts forward to an x/c of approximately 3% and a frequency of 20,000 Hz. Therefore, the above results (Fig. 9-11) demonstrate that a decrease in Reynolds number yields higher shear stresses in the boundary-layer which act to damp out the crossflow instabilities and delay transition. This result corresponds to how suction devices work. Suction on the wing surface thins the boundary layer lowering the effective Reynolds number; and moves the crossflow boundary-layer profile closer to the higher viscous wall region, thereby damping out crossflow instability and extending laminar flow.[6]

Angle of Attack Effects

Effects on predicted transition due to angle of attack at 48% semispan are shown in the boundary-layer stability curves of Fig. 12. The results for the angle-of-attack case of 0 degs indicate that the most unstable frequency is 14000 Hz, and the earliest transition location occurs at an approximate x/c value of 12.25%. The 5 deg angle-of-attack case results show that transition moves back to approximately 18.5% chord at a critical frequency of 12000 Hz. However, the 10 deg case shows that the transition moves only back to 15.75% chord at a critical frequency of 14000 Hz. Therefore, this shows that for an increase in angle of attack, transition moves aft and that certain angles of attack produce more delay in transition than others.

Next, the surface flow patterns of the different angle-of-attack cases near the leading edge at 48% semispan are shown in Fig. 13. The dashed lines indicate the flow trace over the upper wing surface, including the leading-edge point, and the solid lines indicate the flow trace over the lower wing surface. From this plot it is evident that the flow attachment point moves below the leading edge onto the lower surface of the wing as angle of attack increases. It should also be noted from Fig. 13 that as the attachment point rotates below the leading edge, due to the increase in angle of attack, the crossflow velocities on the upper surface of the wing are reduced.

The above attachment line results are confirmed by the findings in a previous parametric study of the F-16XL leading edge attachment line.[12] The F-16XL study showed that the maximum crossflow velocity, at a given wing location, decreased as the angle of attack increased due to the rotation of the attachment point underneath the leading edge. However, the direct effect on transition due to the attachment line and maximum crossflow with changes in angle of attack were not studied in detail. The findings of this current study show that transition can be delayed on the upper surface of the wing as angle of attack is increased for the specific wing geometry and flow conditions considered.

To further investigate the above results, boundary-layer crossflow profile curves are shown in Fig. 14 for the three angle-of-attack cases at approximately mid-semispan (48% semispan). The boundary-layer profile curves are plotted for x/c of 1, 10 and 21%.

Results of the crossflow profiles reveal that the crossflow velocity components are larger for the higher angle-of-attack cases near the leading edge. However, further downstream the trend reverses and the lower angle-of-attack cases exhibit higher crossflow values. In order to better represent this trend, a plot of the maximum crossflow "$(W/U_\infty)max$" versus "x/c" for the different angles of attack is shown in Fig. 15. This plot shows that the maximum crossflows are larger for the higher angles of attack (5 and 10 degs) up to approximately 5% chord. After 5% chord the maximum crossflows for the 5 deg angle-of-attack case fall below the 0 deg angle-of-attack case. The 10 deg angle-of-attack case falls below the 0 deg angle-of-attack case at approximately 8% chord and falls below the 5 deg angle-of-attack case after 16% chord. Finally, the maximum crossflow for the 0 deg angle-of-attack case slowly decreases but remains larger than the two higher angle-of-attack cases after 5% chord.

In summary, increasing angle of attack shows that the maximum crossflow is larger for the higher angles of attack near the leading edge. However, further downstream, near the transition region, the lower angle-of-attack cases exhibit higher maximum crossflow. This correlates with the 6.25% chord increase in laminar flow as the wing's angle of attack is increased to 5 degs and a 3.5% chord increase for the 10 deg case. These results demonstrate that transition appears to be directly influenced by the maximum crossflow in the boundary layer which is discussed further in the next section.

Reynolds Number Effects with Angle of Attack

The results of the previous angle-of-attack cases indicate that maximum crossflow may have a direct influence on the stability of the boundary layer and hence the predicted transition location. To investigate this possibility further, another angle-of-attack study at a different Reynolds number was conducted to see how transition is affected with changes in angle of attack. The 12.7 million Reynolds number flow was used since earlier results indicate that the predicted transition location occurs at nominally 9% chord, forward of the predicted transition location for the 6.8 million Reynolds number flow (Fig. 11). The effect of maximum crossflow on the transition location is now compared with the previous angle-of-attack findings.

A plot of maximum crossflow versus chordwise x/c location for the three angles of attack of 0, 5, and 10 degs at the higher Reynolds number of 12.7 million are shown in Fig. 16. The results show that the maximum crossflow is larger for the higher angles of attack near the leading edge. Further downstream the maximum crossflow is larger for the lower angle-of-attack cases. These trends are similar to those found in the previous lower Reynolds number angle-of-attack cases (Fig. 15).

The boundary-layer stability results (Fig. 17) now predict that transition moves forward as angle of attack is increased. Recall that the results for the lower Reynolds number cases showed the opposite trend (Fig. 12). However, as found in the Reynolds number study, the transition location at 0 deg angle of attack, occurs at 12% chord for the 6.34 million Reynolds number flow and 3% for the 12.68 million Reynolds number flow (Fig. 11). Now referring to the maximum crossflow results for both Reynolds number angle-of-attack cases (Figs. 15 and 16) it is shown that the maximum crossflows near 3% chord increase as the angle of attack increases, and at 12% chord the maximum crossflow decreases as the angle of attack increases. Therefore the transition prediction results (Figs. 12 and 17) along with the maximum crossflow results (Figs. 15 and 16) reveal that the boundary layer can be stabilized as the maximum cross flow in the boundary layer decreases and de-stabilized as the maximum crossflow in the boundary layer increases.

Sweep Effects

In addition to investigating the effects of angle of attack, the effects of sweep were also studied. The results of the maximum crossflow "$(W/U_\infty)max$" at 48% span (Fig. 18) show that maximum crossflow is larger for the higher 60 deg swept wing for all "x/c" except very near the leading edge. Transition results of the sweep study, at 48% semispan (Fig. 19), show that the predicted transition occurs at an x/c of approximately 12% and a frequency of 14,000 Hz for the 45 deg sweep case, and at an x/c of approximately 10% and a frequency of approximately 20,000 Hz for the 60 deg sweep case. Therefore, these results also show that, for sweep effects, maximum crossflow has a direct influence on transition prediction as found in the earlier angle-of-attack results above.

Conclusions

A parametric study to investigate the effects of Reynolds number, angle of attack, and leading-edge sweep on the extent of laminar flow over the upper surface of a generic swept-back wing has been performed. From this study an automated process of predicting transition was developed which substantially decreases the amount of user interactive time from days to a matter of hours.

The results of the Reynolds number study show that a decrease in Reynolds number increases the amount of laminar flow over the wing. This is attributed to the higher shear stress in the boundary layer which acts to damp out the crossflow instabilities, thereby increasing the extent of laminar flow.

The results of the angle of attack study reveal that an increase in angle of attack moves the attachment point beneath the leading edge of the wing increasing the

maximum crossflow near the leading edge and decreasing the maximum crossflow velocities further downstream. The results of the combined effects of Reynolds number and angle of attack show that a direct relationship exists between the maximum crossflow of the boundary layer and the stability of the boundary layer. These results further show that transition can be delayed with an increase in angle of attack for specific Reynolds numbers. The result is an increase in the laminar flow over the wing and a reduction in the viscous drag on the wing. An advantage to this type of natural laminar flow (NLF) control is that the drag increase due to lift (caused by the increase in angle of attack) can partially be recovered by the viscous drag reduction due to the increase in the laminar flow over the wing. The results of the sweep study support the maximum crossflow relation to the boundary-layer stability and hence to the transition prediction.

Finally, detailed boundary-layer comparisons between the Navier-Stokes flow solver (CNS) and the boundary-layer code (WING) identified significant sensitivities to the numerical dissipation of the CNS solutions. A Future detailed investigation into the effects of numerical dissipation in the mean flow predictions is planned.

References

1. Fischer, M. C. and Ash, Robert L., "A General Review of Concepts for Reducing Skin Friction, Including Recommendations for Future Studies," NASA TM X-2894, March 1974.

2. Beckwith, I. E., "Development of High Reynolds Number Quiet Tunnel for Transition Research," AIAA Journal, Vol. 13, No. 3, March 1975, pp. 300-306.

3. Pfenninger, W., "USAF and Navy Sponsored Northrop LFC Research Between 1949 and 1967," in Workshop on Laminar Flow Control, compiled by C. T. D'Aiutolo, NASA Langley Research Center, April 6-7, 1976, pp. 14-50.

4. Malik, M. R., "Stability Theory for Laminar Flow Control Design," Progress in Astronautics and Aeronautics, Vol. 123, 1990, pp. 3-46.

5. Morkovin, M. V., "Critical Evaluation of Transition from Laminar to Turbulent Shear Layer with Emphasis on Hypersonically Traveling Bodies," NTIS AD-686178, 1969,

6. Srokowski, A. J., "Mass Flow Requirement for LFC Wing Design," AIAA Paper 77-1222, Aug. 1977.

7. Kaynak, U., Holst, T. L., and Cantwell, B. J., "Computational of Transonic Separated Wing Flow Using an Euler/Navier-Stokes Zonal Approach," NASA TM 88311, July 1986.

8. Kaups, K., and Cebeci, T., "Compressible Laminar Boundary Layers with Suction on Swept and Tapered Wings," Journal of Aircraft, Vol. 14, No. 7, July 1977, pp. 661-667.

9. Malik, M. R., "COSAL: A Black-Box Compressible Stability Analysis Code for Transition Prediction in Three Dimensional Boundary Layers," NASA Contractor Report 165925, 1982.

10. Beam, R., and Warming, R. F., "An Implicit Finite-Difference Algorithm for Hyperbolic Systems in Conservation-Law Form," Journal of Comp. Physics, Vol. 22, Sept. 1976, pp. 87-110.

11. Pulliam, T. H., "Euler and Thin-Layer Navier Stokes Codes: ARC2D, and ARC3D," Notes for the Computational Fluid Dynamics Users' Workshop, The University of Tennessee Space Institute, Tullahoma, Tenn., Mar. 12-16, 1984.

12. Flores, J., Tu, E. L., Anderson, B., and Landers, S., "A Parametric Study of the Leading Edge Attachment Line for the F-16XL," AIAA Paper 91-1621, Proceedings of the AIAA 22nd Fluid Dynamics, Plasma Dynamics & Laser Conf., Honolulu, Hawaii, June 1991.

13. Keller, H. B., "A New Difference Scheme for Parabolic Problems," Numerical Solutions of Partial Differential Equations, Vol. II, edited by J. Bramble, Academic Press, New York, 1970.

14. Cebeci, T., and Bradshaw, P., Momentum Transfer in Boundary Layers, Hemisphere and Mc Graw Hill, 1977.

15. Keller, H. B., and Cebeci, T., "Accurate Numerical Methods for Boundary Layers. II. Two-Dimensional Turbulent Flows," AIAA Journal, Vol. 10, Sept. 1972, pp. 1197-1200.

16. Cebeci, T., and Smith, A. M. O., Analysis of Turbulent Boundary Layers, Academic Press, New York, 1974.

17. White, F. M., Viscous Fluid Flow, 2nd ed., Mc Graw-Hill Series in Mechanical Engineering, 1991.

18. Chen, F.-J., Malik, M. R., and Beckwith, I. E., "Boundary-Layer Transition on a Cone and Flat Plate at Mach 3.5," AIAA Journal, Vol. 27, No. 6, June 1989, pp. 687-693.

19. Cattafesta III, L.N., Iyer, V., Masad, J. A., King, R. A., and Dagenhart, J. R., "Three-Dimensional Boundary-Layer Transition on a Swept Wing at Mach 3.5," AIAA Paper 94-2375, Proceedings of the 25th AIAA Fluid Dynamics Conference, Colorado Springs, Colorado, June 20-23, 1994.

20. Malik, M. R., "Efficient Computation of the Stability of Three-Dimensional Compressible Boundary Layers," AIAA Paper 81-1277, Palo Alto, California, June 1981.

21. Garcia, J. A., "Parametric Study on Laminar Flow for Finite Wings at Supersonic Speeds," NASA Technical Memorandum 108852 December 1994.

22. Chan, W. M., and Steger, J. L., "A Generalized Scheme For Three-Dimensional Hyperbolic Grid Generation," AIAA Paper 91-1588, Proceedings of the AIAA 10th Computational Fluid Dynamics Conference, Honolulu, Hawaii, 1991.

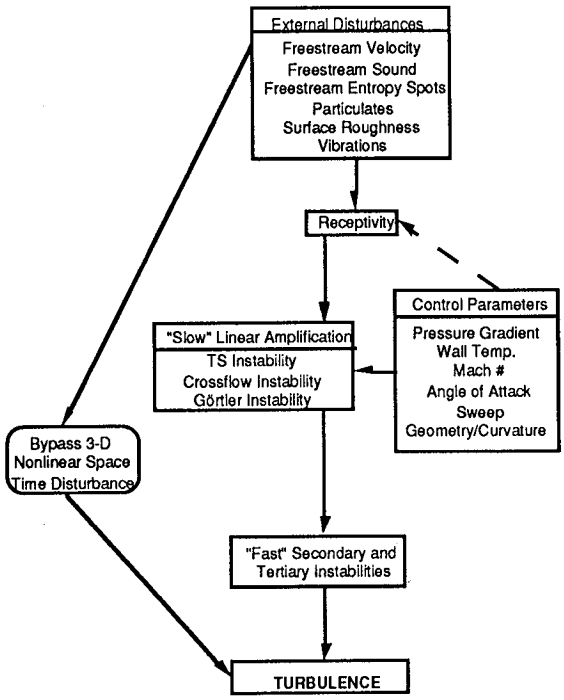

Fig. 1 Transition flow chart. (taken from Ref. 1)

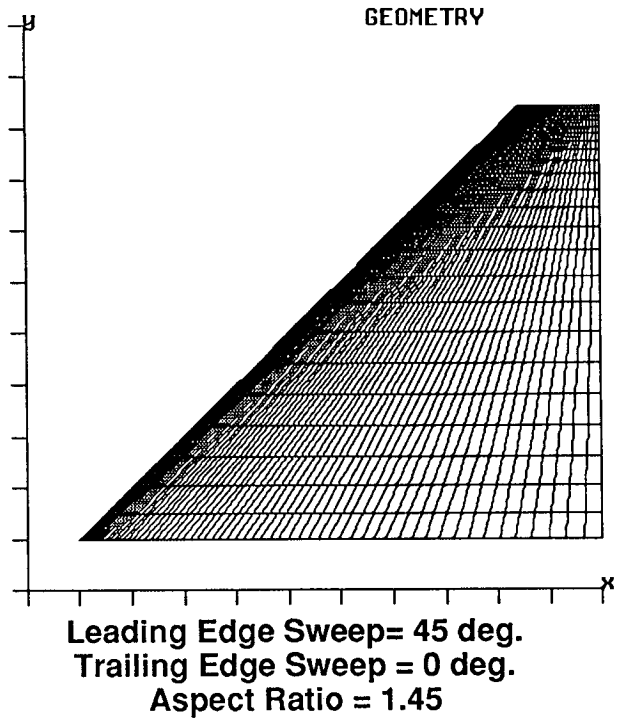

Fig. 2 Swept geometry surface grid. (mesh size is 157x46x75).

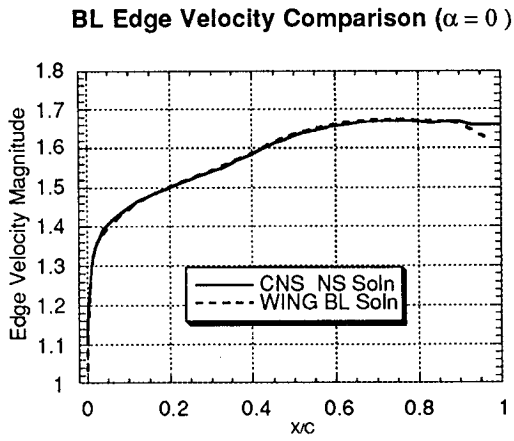

Fig. 3 Boundary Layer Edge Velocity magnitude comparison at 48% semispan.

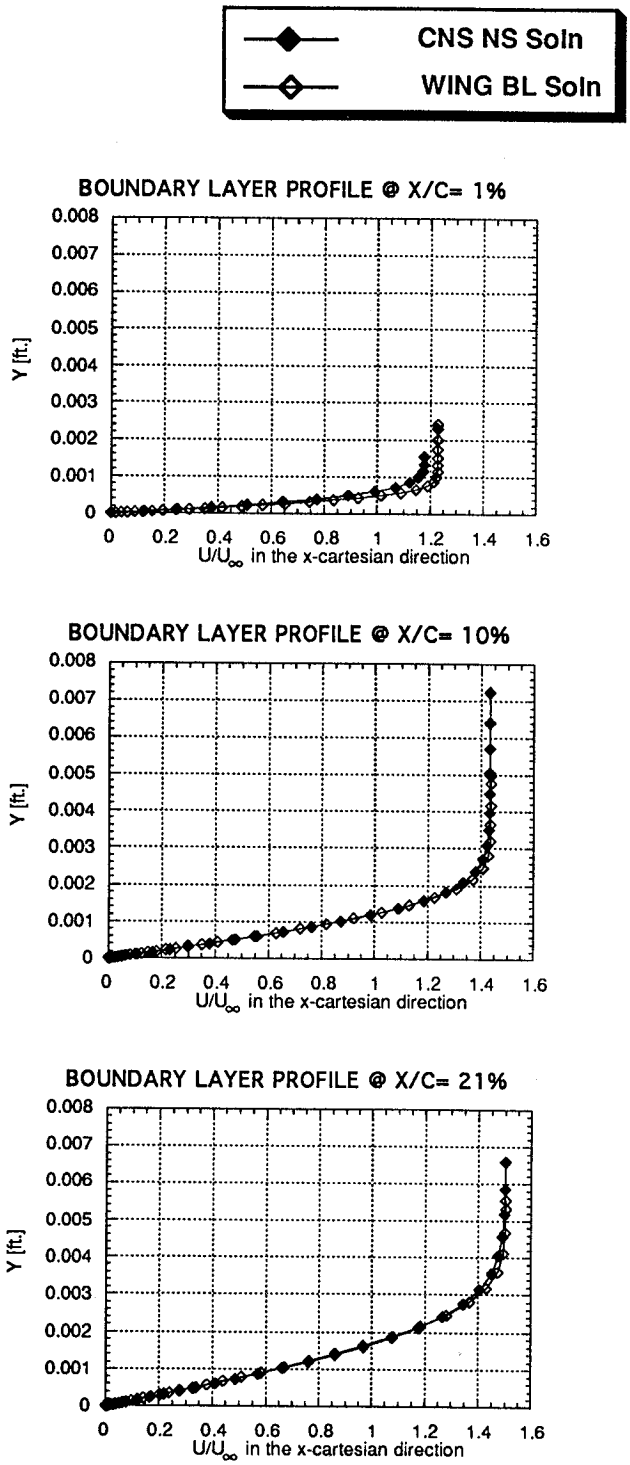

Fig. 4 Boundary Layer velocity profile comparison in the x-Cartesian direction at 48% semispan.

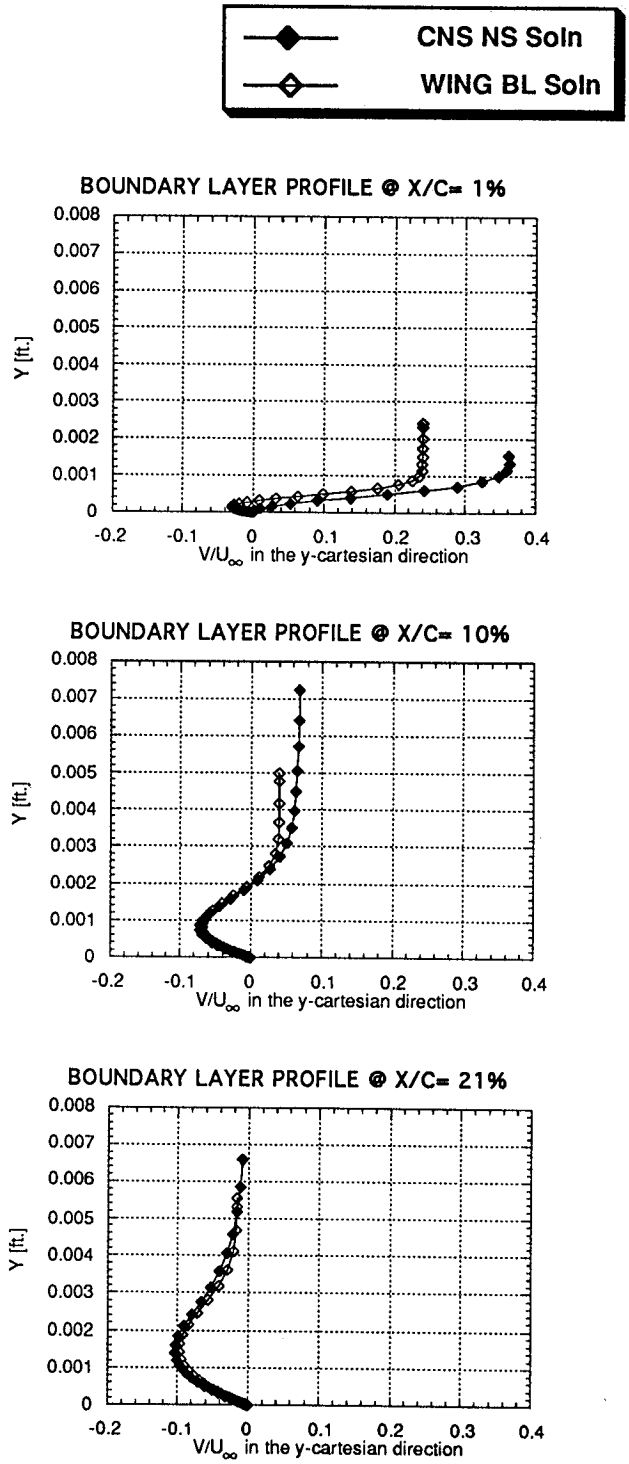

Fig. 5 Boundary Layer velocity profile comparison in the y-Cartesian direction at 48% semispan.

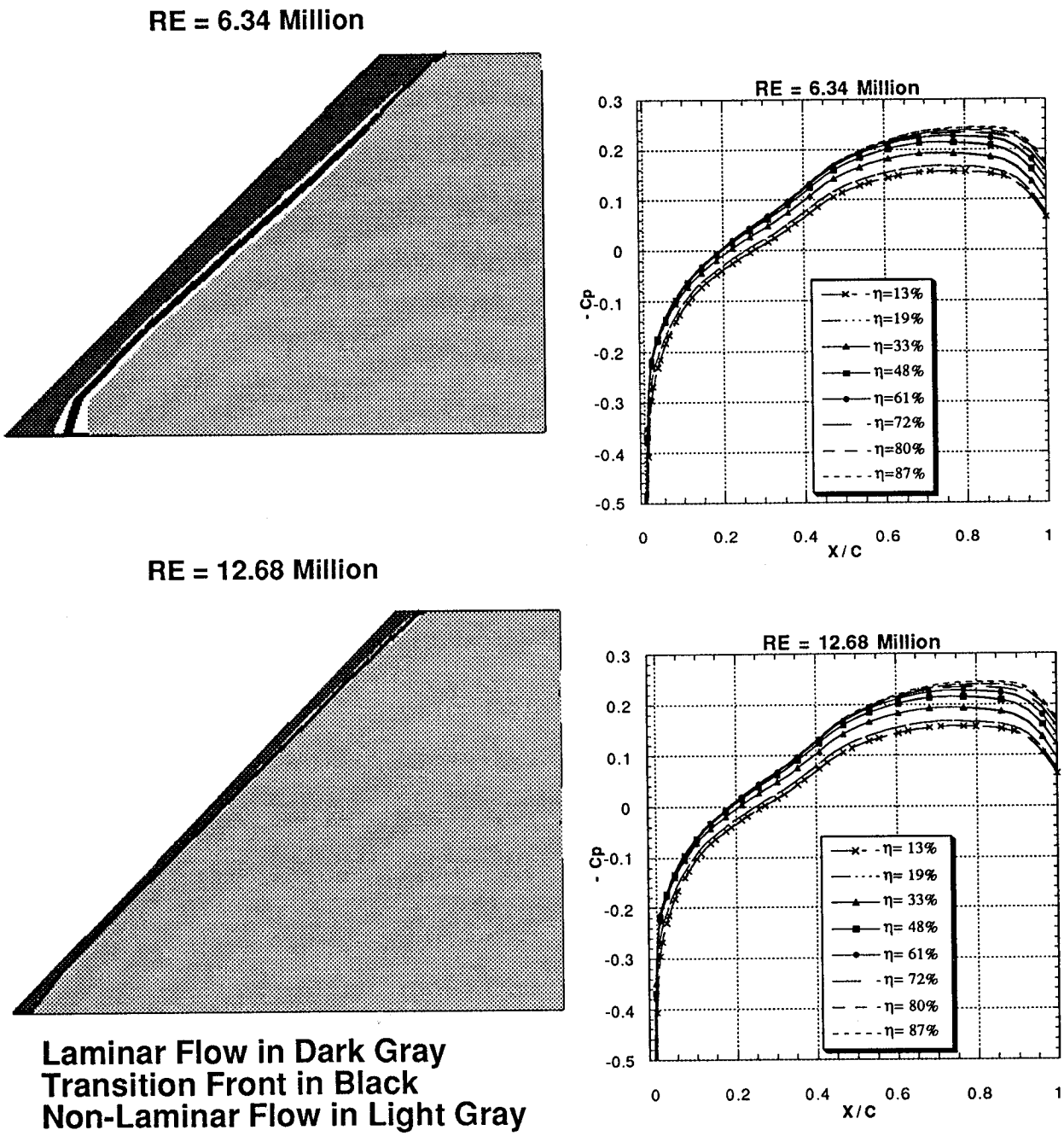

Fig. 6 Effect of Reynolds number on Transition front.

Fig. 7 Chordwise pressure distribution. [α=0°]

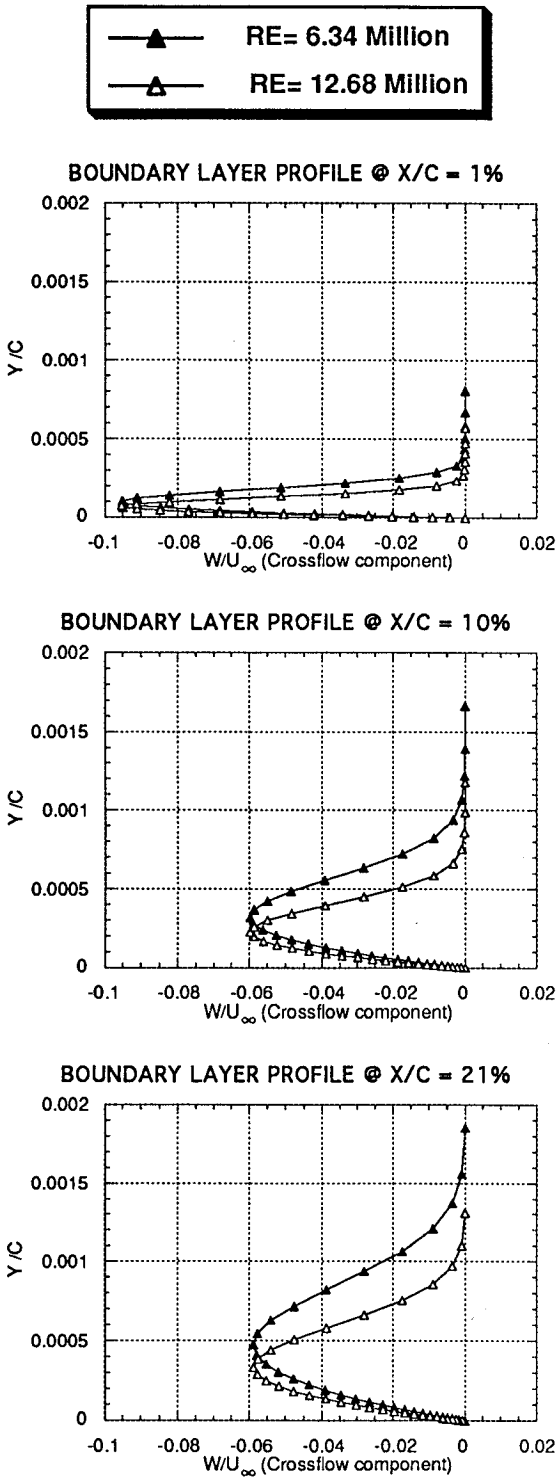

Fig. 8 Effect of Reynolds number on crossflow @48% semispan.

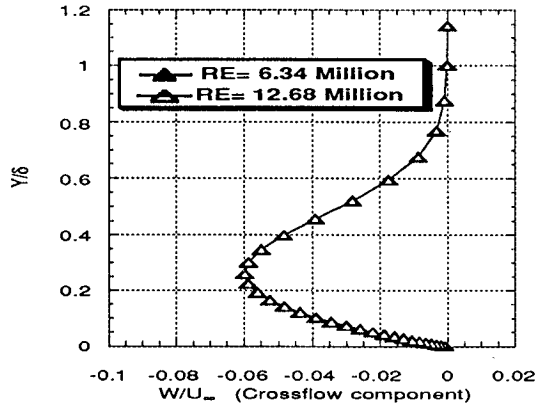

Fig. 9 Effect of Reynolds number on normalized crossflow @48% semispan for x/c=10%.

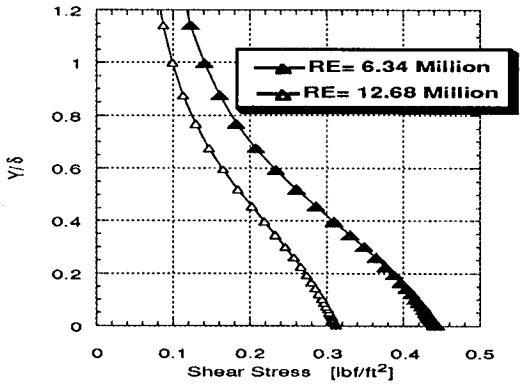

Fig. 10 Effect of Reynolds number on shear stress @48% semispan for x/c=10%.

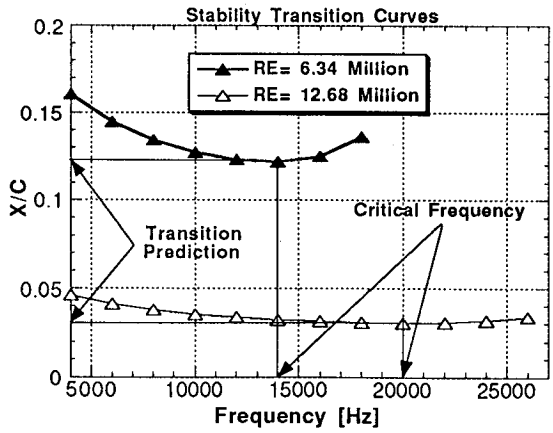

Fig. 11 Effect of Reynolds number on transition @48% semispan.

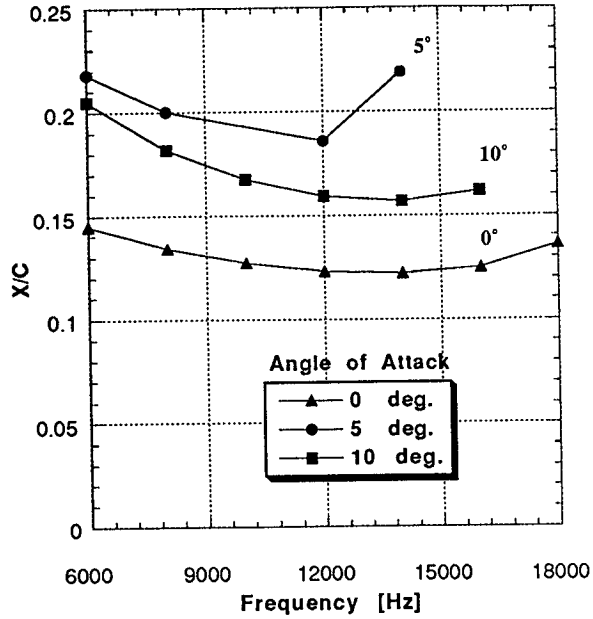

Fig. 12 Effect of angle of attack on transition prediction @48% semispan for Re=6.34 million and 45° sweep.

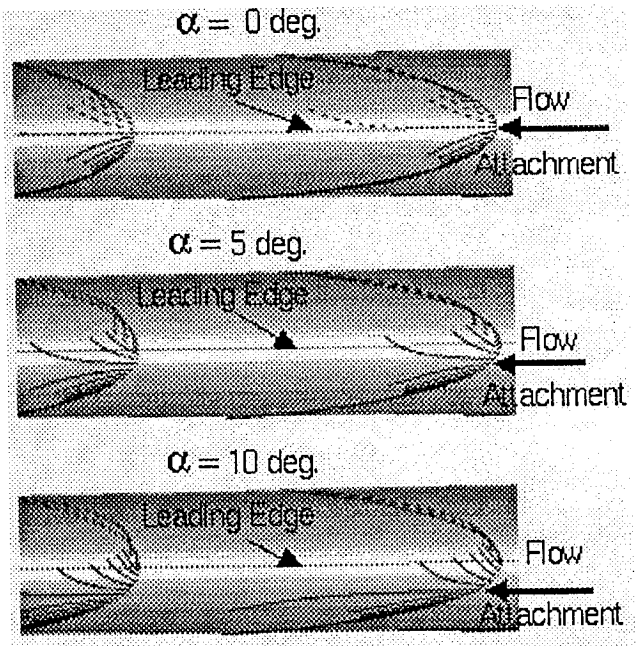

Fig. 13 Effect of angle of attack on leading edge flow attachment @48% semispan.

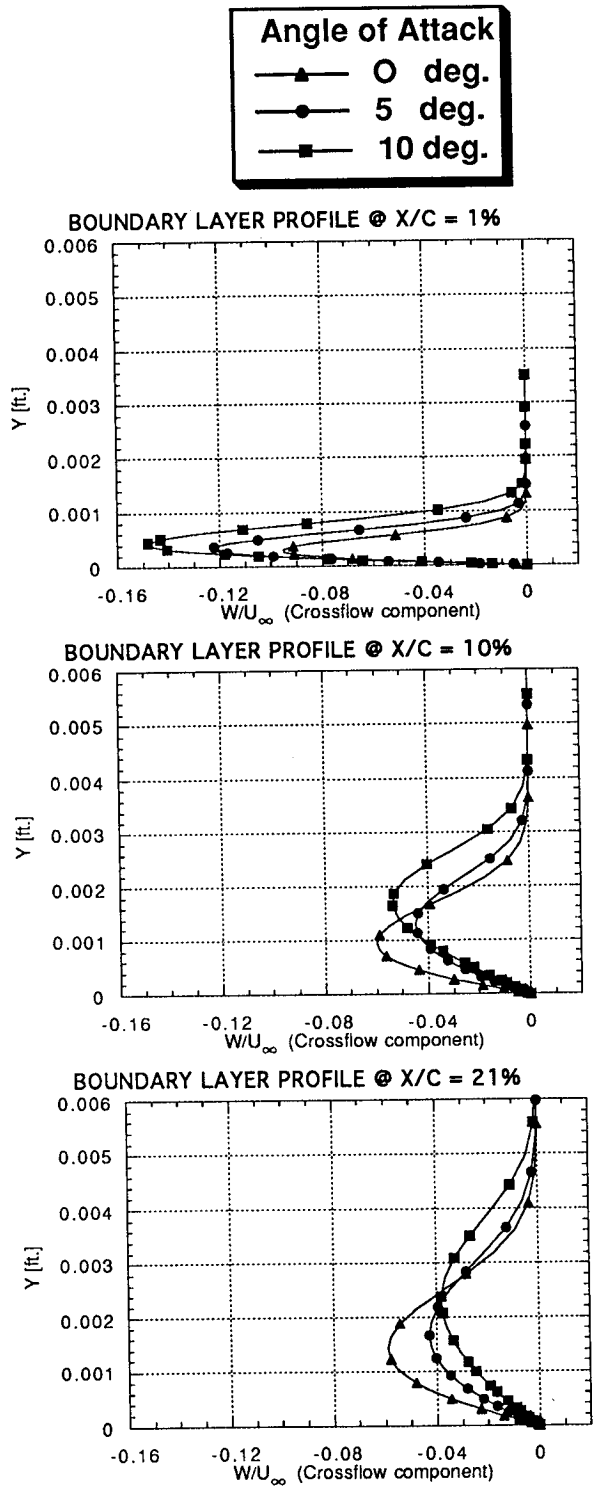

Fig. 14 Effect of angle of attack on crossflow profiles @48% semispan for Re=6.34 million and 45° sweep.

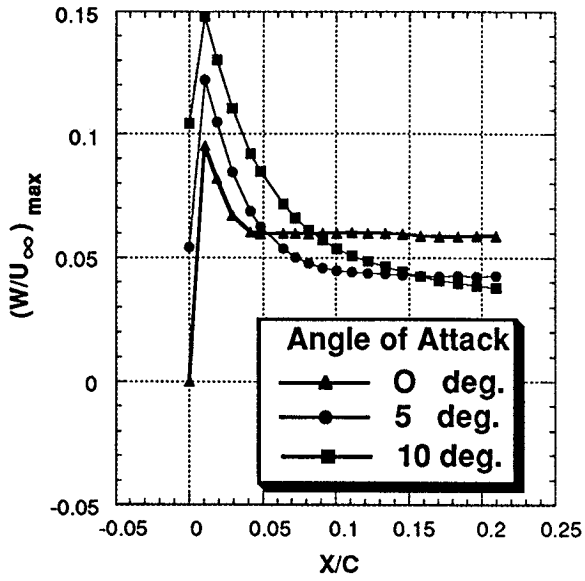

Fig. 15 Effect of angle of attack on maximum crossflow @ 48% semispan for Re=6.34 million and 45° sweep.

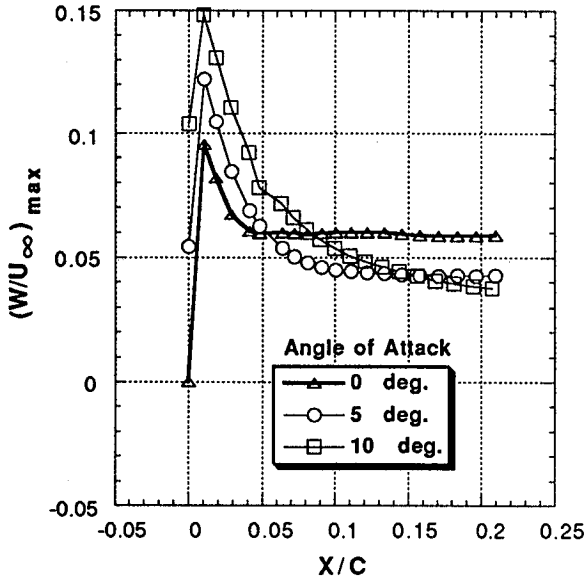

Fig. 16 Effect of angle of attack on maximum crossflow @ 48% semispan for Re=12.68 million and 45° sweep.

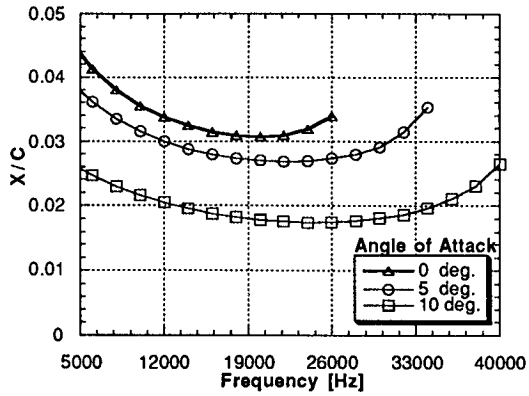

Fig. 17 Effect of angle of attack on transition @48% semispan for higher Re=12.68 million and 45° sweep.

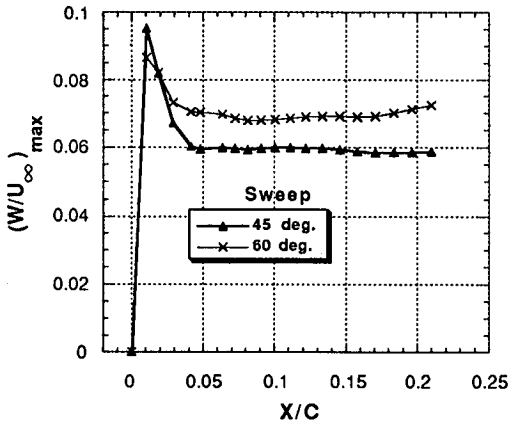

Fig. 18 Effect of leading edge sweep on maximum crossflow @48% semispan for Re= 6.34 million and α=0°.

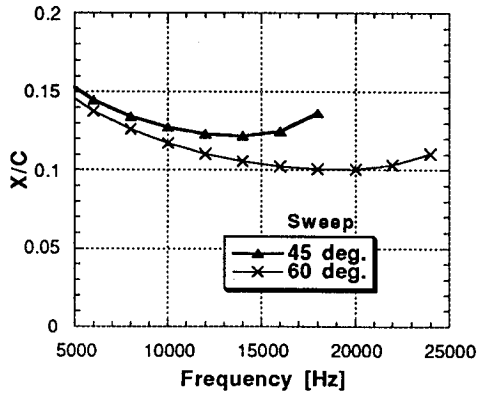

Fig. 19 Effect of leading edge sweep on transition @48% semispan for Re= 6.34 million and α=0°.

NOTES

NOTES